Received: 13 July 2016 | Accepted: 1 February 2017

DOI: 10.1111/jace.14830

ORIGINAL ARTICLE

Journal of the American Ceramic Society

Structure and energetics of SiOC and SiOC-modified carbon-bonded carbon fiber composites

Min Niu[1,2] | Hongjie Wang[1] | Jiewei Chen[2] | Lei Su[1] | Di Wu[2] | Alexandra Navrotsky[2]

[1]State Key Laboratory for Mechanical Behavior of Materials, Xi'an Jiaotong University, Xi'an, China

[2]Peter A. Rock Thermochemistry Laboratory and NEAT ORU, University of California Davis, Davis, California

Correspondence
Hongjie Wang, State Key Laboratory for Mechanical Behavior of Materials, Xi'an Jiaotong University, Xi'an, China.
Alexandra Navrotsky, Peter A. Rock Thermochemistry Laboratory and NEAT ORU, University of California Davis, Davis, CA
Emails: hjwang@mail.xjtu.edu.cn and anavrotsky@ucdavis.edu

Funding information
National Natural Science Foundation of China, Grant/Award Number: 51272206; National Basic Research Program of China, Grant/Award Number: 2015CB655200; Fundamental Research Funds for the Central University, Grant/Award Number: xkjc2014009; China Scholarship Council, Grant/Award Number: 201506280144; U.S. Department of Energy; Office of Science; Office of Basic Energy Sciences, Grant/Award Number: 4000134953

Abstract

The incorporation of SiOC polymer-derived ceramics into porous carbon materials could provide tailored shapeable, mechanical, electrical, and oxidation-resistant properties for high-temperature applications. Understanding the thermodynamic and kinetic stability of such materials is crucial for their practical application. We report here the dependence of structures and energetics of SiOC and SiOC-modified carbon-bonded carbon fiber composites (CBCFs) on the pyrolysis temperature using spectroscopic methods and high-temperature oxide melt solution calorimetry. The results indicate that a SiOC ceramic pyrolyzed at 1200°C and 1600°C is energetically stable with respect to an isocompositional mixture of cristobalite, silicon carbide, and graphite by 4.9 and 10.3 kJ/mol, respectively, and more energetically stable than that pyrolyzed at 1450°C. Their thermodynamic stability is related to their structural evolution. SiOC-modified CBCFs become energetically less stable with increasing preparation temperature and concomitant increase in excess carbon content.

KEYWORDS
silicon oxycarbide, structure, thermodynamics

1 | INTRODUCTION

SiOC polymer-derived ceramics (PDCs) have attracted enormous attention for years due to a variety of unique and superior properties, including excellent thermal stability in oxidative and corrosive environments,[1] high strength and creep resistance,[2,3] and unusual electric behavior.[4] However, fabrication of porous SiOC in a stable shape poses considerable challenge due to the difficulties of keeping the materials undamaged during drying and pyrolysis. Carbon-bonded carbon fiber composites (CBCFs) are a special kind of carbon-carbon composites with low densities (0.1-0.5 g/cm^3) and high porosities (70%-90%), and are constructed by layered carbon fiber networks in which the fibers are bonded together at their intersections by discrete pyrolytic carbon.[5,6] CBCFs are of great importance for high-temperature applications, such as thermal insulation and lightweight structural components.[7,8] However, their application is limited by oxidation of carbon above 450°C. Incorporation of SiOC into the highly porous CBCFs is a double winning strategy, not only can it control shape, but also it can provide tailored electrical, mechanical, and oxidation-resistant properties.[9] Therefore, fundamental understanding of structural evolution and thermodynamic stability of the SiOC and SiOC-modified CBCFs is crucial for their high-temperature applications.

Early work on the microstructure of SiOC ceramics strongly suggested that they are X-ray amorphous at large scale, but heterogeneous at the nanometer length scale.[10,11] Typically, amorphous SiOC consists of SiO_2-rich domains and sp^2 carbon regions intergrown in a complex microstructure. The silica domains, especially in the interfacial regions near the carbon layers contain various mixed tetrahedral units of $SiO_{4-n}C_n$, where n=1, 2, or 3.[12] However, this structure is not stable under high temperature as it undergoes crystallization, irreversible phase separation, and carbothermal reduction of silica to SiC above 1200°C or higher.[13,14] In general, the nanoscale structure of SiOC is sensitively reflected in the number, type, and strength of chemical bonds and the short-, mid-, and long-range order as a function of temperature and composition.

Thermodynamic properties are macroscopic manifestations of these configurations and nanostructures. In particular, the formation enthalpy reflects the overall energetic features of various bonds. It has been reported that amorphous SiOC is energetically stable with respect to an isocompositional mixture of cristobalite, silicon carbide, and graphite, especially when the SiOC is pyrolyzed at 1000°C-1200°C.[12,15,16] The mixed bonding between silicon, oxygen, and carbon and the possible presence of hydrogen in the interfacial regions play a key role in the thermodynamic stabilization of these SiOC materials.[12] In view of the complex structural evolution of SiOC and competing factors including, but not limited to, greater number and stabilization of mixed bonds in the interfacial regions at lower temperature vs the growth of thicker and more stable carbon layers at higher temperature,[11] additional thermodynamic studies are needed to provide a more systematic and complete picture of these and other factors driving the evolution of thermodynamic properties.

In our previous work, SiOC has been incorporated into the highly porous CBCFs by forming SiOC coatings on the surface of carbon fibers.[17] The coating is 0.6-0.8 μm in thickness, while the carbon fiber is 9-11 μm in diameter, indicating the existence of a large amount of excess carbon in the SiOC-modified CBCFs. During high-temperature heat treatment, carbon could enter into reaction with SiOC and form part of the ceramic coating.[18] The interaction between the excess carbon and the coating has great influence on the coating morphologies and structures at different temperatures, which may induce fundamental changes in their thermodynamic properties.

Here we report the structure evolution and thermodynamic properties of SiOC and SiOC-modified CBCFs prepared at 1200°C, 1450°C, and 1600°C. Structural techniques including X-ray diffraction (XRD), Fourier transform infrared (FTIR) spectroscopy, nuclear magnetic resonance (NMR), and Raman scattering were used to study the atomic structure of the ceramics. High-temperature oxidative drop solution calorimetry in a molten oxide solvent was used to examine their thermodynamic properties. Energetics has been interpreted in terms of structural factors. Particular emphasis is given to the previously unexplored structure and energetics of the SiOC pyrolyzed at high temperature (above 1200°C), and to the characterization of the SiOC-modified CBCFs.

2 | EXPERIMENTAL PROCEDURES

Polysiloxane sol was prepared by cohydrolysis of dimethoxydimethylsilane (DMDMS, $(CH_3)_2Si(OCH_3)_2$, ≥98% purity, Meryer Chemical Technology Co., Ltd., Shanghai, China) and methyltrimethoxysilane (MTMS, $CH_3Si(OCH_3)_3$, ≥98% purity, Meryer Chemical Technology Co., Ltd.). DMDMS and MTMS were mixed in the weight ratio of 1:5 with 10 wt.% ethanol as solvent in a stoichiometric amount of water. HNO_3 (0.1N) was added to catalyze the gelation process. The solutions were ultrasonicated in a bath sonicator for ~30 minutes to reach a homogeneous state. The reactions were carried out for 24 hours in air at room temperature until a bulk white gel was obtained after complete polymerization of the solution. All the gel polysiloxanes were ball milled into powders, and then placed on graphite paper in a cylindrical graphite crucible. Pyrolysis was carried out in a graphite furnace with the gas pressure initially pumping down to 0.01 Pa and then raised to 0.25 MPa with high purity (>99.99%) argon gas. These powders were heated at 5°C/min to 1200°C, 1450°C, and 1600°C with an additional 1 hour dwell period at each of the temperatures.

CBCF cubes 5 mm on a side were cut from bulk anisotropic composites with densities of 0.24 ± 0.05 g·cm^{-3} and porosities of 82%-85%. They were cleaned in acetone and ethanol followed by oven drying at 100°C for 6 hours. The samples were dipped in the polysiloxane sol with a viscosity of 7-8 mPa·s under vacuum. Excess sol stacked in the holes constructed by carbon fibers was removed by centrifugation. After gelation for 24 hours in air at room temperature, the samples were heated in graphite crucibles to 1200°C, 1450°C, and 1600°C in the same way as the gel powders. Six different samples are labeled as S1200, S1450, S1600, CS1200, CS1450, and CS1600. The numbers represent pyrolysis temperatures.

Elemental analysis for Si and C was performed by a titration method using K_2SiF_6 and by a high-frequency combustion infrared absorption method (HF-2000; Xixin Precision Instruments Co., Ltd., Shanghai, China), and the balance of mass was assumed to be oxygen. Oxygen content was determined by N/O analyzer (LECO TC-436, LECO, St. Joseph, MI, USA). The difference between the values calculated and the experimental results are within

the errors of the measurement. H content was measured by combustion/LECO TCH600 method, and was found below the detectable limit which is less than 0.3 wt.%. The analysis was repeated three times by two different operators for reproducibility. Phase composition of samples was characterized by a powder XRD (X'Pert PRO, PANalytical, Almelo, Holland) instrument using CuK_α radiation (40 kV, 40 mA). The scans were acquired in the 2θ range of 10°-90° with a step size of 0.02° using a low-background quartz holder. Chemical structure of samples was examined using FTIR spectroscopy (VERTEX70; Bruker, Karlsruhe, Germany). All spectra were acquired from 400 to 7000 cm^{-1} with 4 cm^{-1} resolution and signal averaged over 128 scans. The Raman spectra were recorded on a Raman Station (HR-800; HORIBA, Jobin Yvon, France) using an Ar-Ion laser with a wavelength of 514.5 nm. Ten spectra were collected for each sample at different positions to minimize errors associated with material heterogeneity. The solid-state ^{29}Si NMR spectra were recorded on a Varian Infinity-plus 400 (Varian, Palo Alto, CA, USA) NMR spectrometer with a commercial double resonance magic angle spinning (MAS) probe at Larmor frequency of 79.47 MHz for ^{29}Si. The MAS speed was 4 kHz in all ^{29}Si direct polarization MAS NMR measurements. Solid-state ^{29}Si NMR spectra were recorded with a single pulse excitation using a short tip angle (*pi*/4) to obtain quantitative results with a pulse length of 4 μs and a recycle delay of 50 seconds. The ^{29}Si chemical shifts were determined using a solid external reference kaolin resonance at −91.5 ppm relative to tetramethylsilane.

High-temperature oxidative drop solution calorimetry was utilized to determine the formation enthalpies of the samples. This method has been applied previously to study SiOC ceramics.[12,15,19] In a typical measurement, pellets about 5.0 mg in mass with diameter of 1 mm were dropped from room temperature into molten sodium molybdate ($3Na_2O{\cdot}4MoO_3$) solvent maintained at 800°C in a platinum crucible inside a custom built Tian-Calvet twin microcalorimeter. Oxygen gas was bubbled through the solvent at ~5 mL/min to accelerate the oxidation reaction rate and stir the melt. The pellets dissolved in the solvent within an hour, and converted to cristobalite and CO_2 as a result of oxidation. The gaseous CO_2 was removed immediately by continuous flushing of oxygen gas at ~25 mL/min through the calorimeter assembly. Multiple runs were performed to ascertain the accuracy and reliability of the data. For the pure CBCFs, approximately 1 mg pellet was dropped from room temperature into a silica glass crucible containing a small piece of silica wool at its bottom in the calorimeter maintained at 800°C. No solvent was used and pellets were rapidly oxidized to CO_2 at the calorimeter temperature. Air was flushed through the area close to the silica wool at 20 mL/min and through the calorimeter assembly at 50 mL/min to ensure complete oxidation of samples to CO_2. Oxygen atmosphere caused the samples to flare during the drop and so air atmosphere was chosen for these experiments to ensure that oxidation of the samples happens only in the calorimeter chamber. The calorimeter was periodically (every 6 weeks) calibrated against the heat content of platinum pellets. Statistically reliable data (within 2% error) were obtained by dropping a number of pellets. This methodology is well established and has been used for other carbon-rich materials.[12,20]

3 | RESULTS

3.1 | Composition and structure

Chemical compositions of S and CS samples are shown in Table 1. S1200 and S1450 have similar composition (given on a gram atom basis-one mole of Si+O+C) of $Si_{0.307}O_{0.461}C_{0.232}$ and $Si_{0.305}O_{0.462}C_{0.233}$, while that of S1600 is $Si_{0.314}O_{0.434}C_{0.252}$. The content of oxygen slightly decreases in S1600 presumably by carbothermal reduction of silica at 1600°C.[14,21] The content of carbon is much higher than required to form stoichiometric silicon carbide, indicating the existence of free carbon. Given that oxygen is mainly bonded to silicon and few, if any, Si–Si bonds exist in the material,[10] the majority of the remaining silicon atoms are thought to be bonded to carbon, thus the free carbon content can be calculated from the apparent formula (Table 1). The free carbon content in the S samples first increases as the pyrolysis temperature increases from 1200°C to 1450°C, and then decreases as the temperature increases to 1600°C, confirming that some of the free carbon is consumed by carbothermal reduction at 1600°C. Chemical composition of CS1200 is $Si_{0.085}O_{0.144}C_{0.771}$, while that of CS1450 and CS1600 is $Si_{0.062}O_{0.002}C_{0.935}$ and $Si_{0.050}O_{0.003}C_{0.947}$. Atomic percentage of carbon in the CS samples increases by 223%-296% in comparison to that in the S samples owing to the CBCF substrate. A tiny amount (<14.4 at.%) of oxygen is detected in the CS

TABLE 1 Chemical compositions of the S and CS samples prepared at 1200°C, 1450°C, and 1600°C

	$Si_aO_bC_c$ (a+b+c=1)			
Samples	***a***	***b***	***c***	**SiC-SiO_2 and free carbon**
S1200	0.307	0.461	0.232	$SiO_{1.50}C_{0.25}{\cdot}0.51C$[a]
S1450	0.305	0.462	0.233	$SiO_{1.52}C_{0.24}{\cdot}0.52C$
S1600	0.314	0.434	0.252	$SiO_{1.38}C_{0.31}{\cdot}0.50C$
CS1200	0.085	0.144	0.771	$SiO_{1.69}C_{0.15}{\cdot}8.92C$
CS1450	0.062	0.002	0.935	$SiO_{0.04}C_{0.98}{\cdot}13.99C$
CS1600	0.050	0.003	0.947	$SiO_{0.07}C_{0.97}{\cdot}17.98C$

[a]Stands for free carbon.

samples, especially for CS1450 and CS1600 (<0.3 at.%). This is because excess carbon in the CS samples provides almost complete reduction of oxygen containing units. In addition, excess carbon content increases with increasing preparation temperature, which is mainly attributed to the decrease of silicon containing units by partial thermal evaporation[22] and thermal reduction of SiOC to form of gaseous SiO and CO at high temperatures.

Figure 1 shows powder XRD patterns of S and CS samples. All S samples exhibit a very broad peak near ~22° which is attributed to noncrystalline silica.[23] No other diffraction peaks are detected for S1200. Small peaks centered at 35.59°, 59.97°, and 71.78° which are indexed to be β-SiC (JCPDS Card No. 00-029-1129) appear in S1450 and become more evident in S1600, indicating crystallization of β-SiC is promoted with increasing temperature. The analysis of line broadening of diffraction peaks, according to the Scherrer equation, allows us to estimate the domain size. The size of the silica domains is approximately 0.8 nm for S1200, 1.2 nm for S1450, and 1.3 nm for S1600, growing slightly with increasing temperature. The silica peak is broad in the three S patterns, indicating that the domain structure remains highly disordered up to 1600°C. It is possible that the formation of SiO_2 critical nuclei for crystallization may be hindered by interior SiC nuclei and turbostratic carbon layers.[24] A shoulder near 26° in the pattern of S1600 (indicated by the down-pointing triangle) is evident. This reflection can be attributed to graphite as well as to turbostratic carbon. In addition, heat treatment above 1200°C yields crystallization of β-SiC. The crystallite size calculated on the (111) peak of β-SiC is 3.4 nm at 1450°C and 4.6 nm at 1600°C. Their growth is also limited by low diffusion. These results are in good agreement with previous reported SiOC PDC.[14,23,25] In the CS pattern, the peak detected at 26.6° is attributed to the (002) reflection of graphitic carbon (JCPDS Card No. 00-008-0415) from the CBCF substrate. By increasing the pyrolysis temperature, carbothermal reduction of silica becomes abundant, and consequently the silica halo observed in CS1200 progressively decreases, allowing the reflections of the crystalline phases (SiC and graphite) present in the CS samples to emerge and become the only diffraction peaks at 1600°C. The diffraction peaks corresponding to β-SiC show stronger intensity and narrower line width in comparison with those in the S samples. Sharp peaks are indicative of highly ordered structure. Excess carbon in the CS samples promotes thermal reduction of silica and crystallization of β-SiC.

The FTIR spectra of S and CS samples prepared at different temperatures are shown in Figure 2. In all spectra, characteristic bands for Si–O and Si–C vibrations are visible. The band located in the range 1000-1300 cm^{-1} is associated with the asymmetric stretching Si–O–Si mode. This band is composed of two transverse optical (TO) resonant modes, an intense one attributed to TO1 Si–O–Si stretching mode at 1090 cm^{-1}, and a shoulder identified as TO2 Si–O–Si stretching mode around 1200 cm^{-1}.[26] The absorption band of Si–C is observed between 747 and 855 cm^{-1}.[25] The Si–C stretching observed is quite weak for S1200 and begins to increase at temperature above 1450°C, owing to the beginning of carbothermal reduction. For CS samples, limited amount of the Si–O–Si bond is detected in CS 1200, and disappears completely for CS1450 and CS1600, indicating that most of the silica is consumed in the carbothermal reduction by excess carbon. Si–C stretching becomes stronger with the increase in temperature.

More detailed information concerning the Si atomic environment for S samples is obtained from the single pulse ^{29}Si MAS NMR spectrum (Figure 3). The spectrum was curve-fitted using five Gaussian peaks with δ_{iso} around −110, −71, −34, 1, and −11 ppm corresponding to the SiO_4, SiO_3C, SiO_2C_2, $SiOC_3$, and SiC_4 structural units, respectively.[27] The percentages of each Si unit in the S samples calculated from the NMR data are listed in Table 2. S1200 contains the highest fractions of SiO_4 and mixed bonded $SiO_{4-n}C_n$ tetrahedra units. The fractions of the mixed bonded units decrease, while those of SiO_4 and SiC_4 units increase when the pyrolysis temperature is

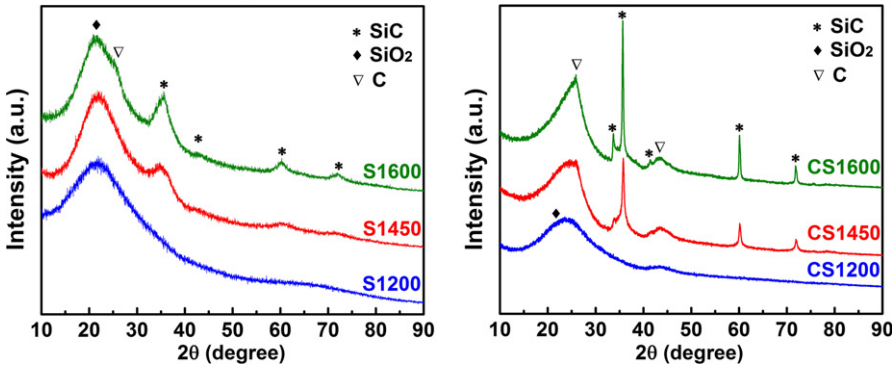

FIGURE 1 XRD patterns of the S and CS samples prepared at 1200°C, 1450°C, and 1600°C, as labeled [Color figure can be viewed at wileyonlinelibrary.com]

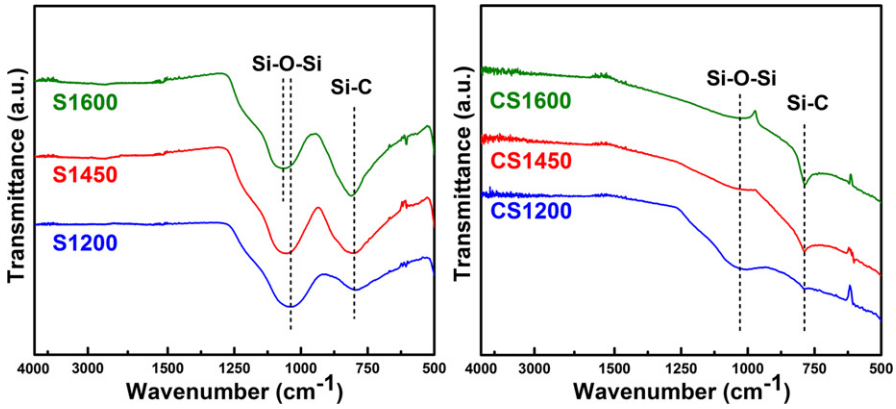

FIGURE 2 FTIR spectra of the S and CS samples prepared at 1200°C, 1450°C, and 1600°C, as labeled [Color figure can be viewed at wileyonlinelibrary.com]

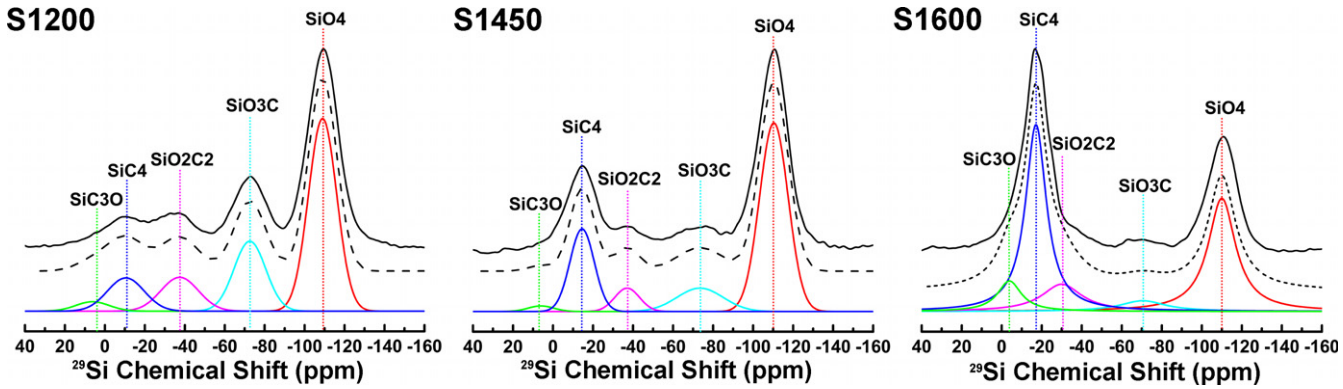

FIGURE 3 ^{29}Si MAS NMR spectra recorded on samples SiOC pyrolyzed at 1200°C, 1450°C, and 1600°C [Color figure can be viewed at wileyonlinelibrary.com]

TABLE 2 Si species found by NMR

Sample	Parameters	SiO_4	SiO_3C	SiO_2C_2	$SiOC_3$	SiC_4
S1200	Position (ppm)	−108.99	−72.57	−37.42	6.21	−10.47
	FWHM (ppm)	16.65	18.75	22.16	19.76	21.70
	Percentage (%)	51.90	21.23	12.15	3.03	11.69
S1450	Position (ppm)	−110.35	−73.47	−37.03	6.05	−14.52
	FWHM (ppm)	16.87	27.21	14.58	15.22	14.25
	Percentage (%)	58.72	11.13	6.29	1.56	21.70
S1600	Position (ppm)	−110.00	−70.50	−30.00	−3.84	−17.11
	FWHM (ppm)	16.61	28.00	24.20	14.33	12.58
	Percentage (%)	33.40	5.33	11.73	7.77	41.78

increased to 1450°C, signifying demixing of the SiOC network. At 1600°C, carbon-rich mixed Si units increases and SiC_4 unites increase at the expense of SiO_4 units. It indicates that carbothermal reduction is strong at 1600°C. The peak position of SiC_4 units shifts from −10.47 to −17.11 ppm, which is due to the formation of crystalline β-SiC with some α-SiC at higher temperature.[28] The concentration of mixed bonds in S1600 is higher than that in S1450. This might be attributed to stronger reactions between free carbon fragments with the surrounding host, and structural disorder of carbon occurs, forming more edges of graphene layers. Carbon atoms can only bond to either other carbon atoms or directly to silicon at high temperatures. Therefore, it is assumed that most of the edges of the graphene layers are bonded to either Si or to oxygen forming mixed $SiO_{4-n}C_n$ units, thus creating some

additional mixed units. SiC_4 units increase with increasing temperature, SiO_4 units first increase and then decrease, while $SiO_{4-n}C_n$ units first decrease and then increase. This trend is consistent with the segregation of the amorphous SiOC network and the formation of crystalline SiC by carbothermal reduction at 1600°C.

The stoichiometric calculations of composition from elemental analysis shows that 61.7-68.4 mol% of the total amount of carbon does not belong to the SiOC network and is present as free carbon in the S samples. Raman spectroscopy was performed to analyze structural evolution of the free carbon phase (Figure 4). The Raman spectrum exhibits two major bands attributed to the D band (~1355 cm^{-1}) and G band (~1608 cm^{-1}) of the free carbon phase, which are assigned to the disordered carbon (turbostratic carbon layers or nanographitic domains) and graphitized carbon (in-plane displacement of carbon atoms in hexagonal carbon sheets), respectively.[25,29] These bands can vary in intensity, position, and width depending on the structural ordering of carbon,[23] and the relative parameters are listed in Table 3. The intensity ratio of D bands and G bands, I_D/I_G, reflects lateral crystallite size, L_a, of the free carbon clusters according to the equation of $\frac{I_D}{I_G} = C'(\lambda)L_a^2$, and where $C'(\lambda)$ is a constant depending on the laser wavelength and is 0.0055 $Å^{-2}$ for the wavelength of 514 nm. It can be calculated that L_a of the carbon clusters increases from 1.67 to 1.77 nm as pyrolysis temperature increases from 1200°C to 1450°C and then decreases to 1.43 nm with further increasing temperature to 1600°C. Increase in the lateral size of the carbon clusters is primarily due to the in-plane growth of the graphite. The lateral size of the carbon clusters increases with increasing free carbon content. The broadening of these bands relates to the degree of structural disorder of the graphitic phase (broad in highly disordered carbons, whereas much more narrow in polycrystalline graphite).[23] FWHM of the two bands decreases as the pyrolysis temperature increases from 1200°C to 1450°C, implying a free carbon phase transformation from amorphous carbon to crystalline graphite. The FWHM then increases from 1450°C to 1600°C due to the appearance of minor peak D' at 1620 cm^{-1}.[31] The 2D band at 2700 cm^{-1} related to the graphitic ordering of carbon appears at 1450°C and becomes evident at 1600°C, indicating the higher graphitization degree of free carbon at 1600°C. While the minor peak D' indicates a disordered graphitic lattice, which could be attributed to the formation of disordered edges of graphene layers through consumption of free carbon by carbothermal reduction. Therefore, it is assumed that the carbon atoms within the graphene layers become more ordered except the ones at their molecular edges.

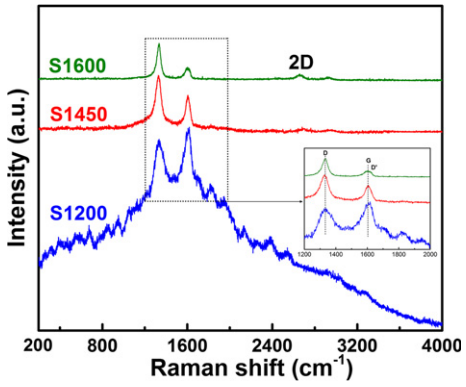

FIGURE 4 The Raman spectrum of S samples pyrolyzed at different temperatures, as labeled [Color figure can be viewed at wileyonlinelibrary.com]

TABLE 3 Evolution of the relative intensity (I_D/I_G), peak frequency (w), and full width at half-maximum (FWHM) of the D and G bands with the pyrolysis temperature

Sample	I_D/I_G	w_D (cm^{-1})	$FWHM_D$ (cm^{-1})	w_G (cm^{-1})	$FWHM_G$ (cm^{-1})
S1200	1.54	1329.3	301.4	1612.5	205.8
S1450	1.73	1355.2	55.1	1608.9	58.8
S1600	1.13	1349.7	99.2	1592.3	110.3

3.2 | Thermochemistry

The measured drop solution enthalpies, ΔH_{ds}, of S and CS samples combined with other known thermodynamic quantities were used to calculate the oxidation enthalpy at 25°C, ΔH_{ox}, the formation enthalpy from corresponding elements, $\Delta H_{f,elem}$, and the enthalpy of formation from components of crystalline silica (cristobalite), silicon carbide, and graphite, $\Delta H_{f,comp}$, through the thermodynamic cycles in Table S1. The enthalpy of formation of CBCF substrate from graphene was obtained using the thermodynamic cycles in Table S2. The obtained values of ΔH_{ox}, $\Delta H_{f,elem}$, and $\Delta H_{f,comp}$ for S, CS, and CBCFs are listed in Table 4.

All the oxidation enthalpies are strongly exothermic, being dominated by the oxidation of carbon. The ΔH_{ox} values of CS are more negative than that of S, which is due to their higher carbon content. The enthalpies of formation from the elements are also strongly negative, which is −219.76±2.87, −209.17±3.14, and −214.34±1.10 kJ/mol for S1200, S1450, and S1600, respectively, indicating S samples are clearly stable with respect to their elemental constituents. Moreover, the SiOC pyrolyzed at 1200°C and 1600°C is energetically more stable than that pyrolyzed at 1450°C. Of particular interest is the enthalpy of formation from the constituents silicon carbide, cristobalite, and graphite, which is −4.92±2.95, 6.13±3.21, and −10.25±1.34 kJ/mol for S1200, S1450, and S1600, respectively. As seen, the value for S1200 and S1600 is exothermic, which means that the SiOC pyrolyzed at 1200°C and 1600°C is energetically stable with respect to

TABLE 4 Enthalpies of drop solution (ΔH_{ds}), enthalpies of oxidation at room temperature (ΔH^0_{ox}, 25°C), enthalpies of formation from elements ($\Delta H^0_{f,\ elem}$), enthalpies of formation ($\Delta H^0_{f,comp}$) from compounds for S and CS obtained at different temperatures, as well as ΔH_{ds}, ΔH^0_{ox}, $\Delta H^0_{f,\ elem}$ from graphite for CBCF

	Atomic percentage						
Sample	Si	O	C	ΔH_{ds} (kJ/mol)	ΔH_{ox} (kJ/mol)	$\Delta H_{f,\ elem}$ (kJ/mol)	$\Delta H_{f,\ comp}$ (kJ/mol)
S1200	30.69	46.07	23.24	–134.22±2.80[a]	–150.49±2.80	–219.76±2.87	–4.92±2.95
S1450	30.49	46.21	23.30	–143.24±3.07	–159.48±3.07	–209.17±3.14	6.13±3.21
S1600	31.37	43.37	25.26	–153.66±0.88	–170.01±0.88	–214.34±1.10	–10.25±1.34
CS1200	8.50	14.37	77.13	–307.88±2.16	–321.22±2.16	–59.51±2.17	6.73±2.17
CS1450	6.25	0.23	93.52	–378.78±1.70	–391.77±1.70	–32.98±1.70	–27.45±1.74
CS1600	5.00	0.34	94.67	–397.84±1.94	–410.67±1.94	–7.23±1.95	–2.17±1.97
CBCF	0	0	100	–217.29±2.68	–229.49±2.68	–164.01±2.68	–

[a]Uncertainty is two standard deviations of the mean.

their crystalline components while that pyrolyzed at 1450°C appears slightly energetically metastable. Nevertheless, because the SiOC samples are amorphous with considerable disorder, it is likely that their entropy of formation from the crystalline constituents is sufficiently positive to give all three a negative free energy of formation from the crystalline constituents. The enthalpy of formation from elements for CS is −59.51±2.17 kJ/mol for CS1200 ($SiO_{1.69}C_{0.15}$·8.92C), −32.98±1.70 kJ/mol for CS1450 ($SiO_{0.04}C_{0.98}$·13.99C), and −7.23±1.95 kJ/mol for CS1600 ($SiO_{0.07}C_{0.97}$·17.98C). These values become less exothermic with increasing preparation temperature and concomitant increase of excess carbon content. In addition, CS samples show less thermal stability than S samples. The enthalpy of formation of CBCFs relative to graphite is −164.01±2.68 kJ/mol.

Thermochemical cycles for CS formed from S and CBCFs at different temperatures are shown in Table S3. The formation equation is balanced using SiO and CO gases. The obtained values of enthalpies of reactions are listed in Table 5. The interaction enthalpies of S1200, S1450, and S1600 with CBCFs become more endothermic with increasing temperature, giving 232.39±3.98, 280.69±3.95, and 305.18±2.80 kJ/mol at 1200°C, 1450°C, and 1600°C, respectively.

TABLE 5 Reaction enthalpies of CS from S and CBCF at different temperatures

Temperature	Reaction	ΔH (kJ/mol)
1200°C	$Si_{0.307}O_{0.461}C_{0.232}$ (solid, 25°C)+ 0.634 CBCF (solid, 25°C)→$Si_{0.085}O_{0.144}C_{0.771}$ (solid, 25°C)+0.222 SiO (gas, 25°C)+0.095 CO (gas, 25°C)	232.39±3.98
1450°C	$Si_{0.305}O_{0.462}C_{0.233}$ (solid, 25°C)+ 0.919 CBCF (solid, 25°C)→ $Si_{0.062}O_{0.002}C_{0.935}$ (solid, 25°C) +0.243 SiO (gas, 25°C)+0.217 CO (gas, 25°C)	280.69±3.95
1600°C	$Si_{0.314}O_{0.434}C_{0.252}$ (solid, 25°C)+ 0.862 CBCF (solid, 25°C)→ $Si_{0.05}O_{0.003}C_{0.947}$ (solid, 25°C)+ 0.264 SiO (gas, 25°C)+ 0.167 CO (gas, 25°C)	305.18±2.80

4 | DISCUSSION

The structural evolution and thermodynamic stability of the SiOC and SiOC-modified CBCFs have been characterized by elemental analysis, XRD, FTIR, ^{29}Si NMR, Raman, and high-temperature oxide melt calorimetry. The structure of these materials undergoes several significant changes with increasing pyrolysis temperature. The calculated formation enthalpies from elements at 25°C for S and CS are exothermic, which suggest they both are thermodynamically stable at room temperature. However, the enthalpy of formation from elements for S1450 is less exothermic than that of S1200 and S1600. The formation enthalpy from elements for CS samples becomes less exothermic as temperature increases, and the values are less negative than those of the S samples. Thermodynamic stabilities of these samples are discussed in relation to their structures below. Our discussion does not consider the influence of hydrogen on the structure and energetics as our samples, after treatment at high temperature, contain negligible *H*.

Energetics of SiOC can be investigated based on their structures in terms of the SiO_2-rich domains, silicon carbide, and the free carbon regions. In our case, SiOC samples are composed of 46.20-49.79 mol% SiO_2 domains, 15.91-20.63 mol% SiC domains, and 33.18-34.29 mol% free carbon. Figure 5 presents the structural evolution of each domain and the interfacial area between them, as well as the dominant factors influencing stabilization and destabilization. In the SiOC network domains, the embedding of disordered SiC clusters in amorphous silica-rich regions increases

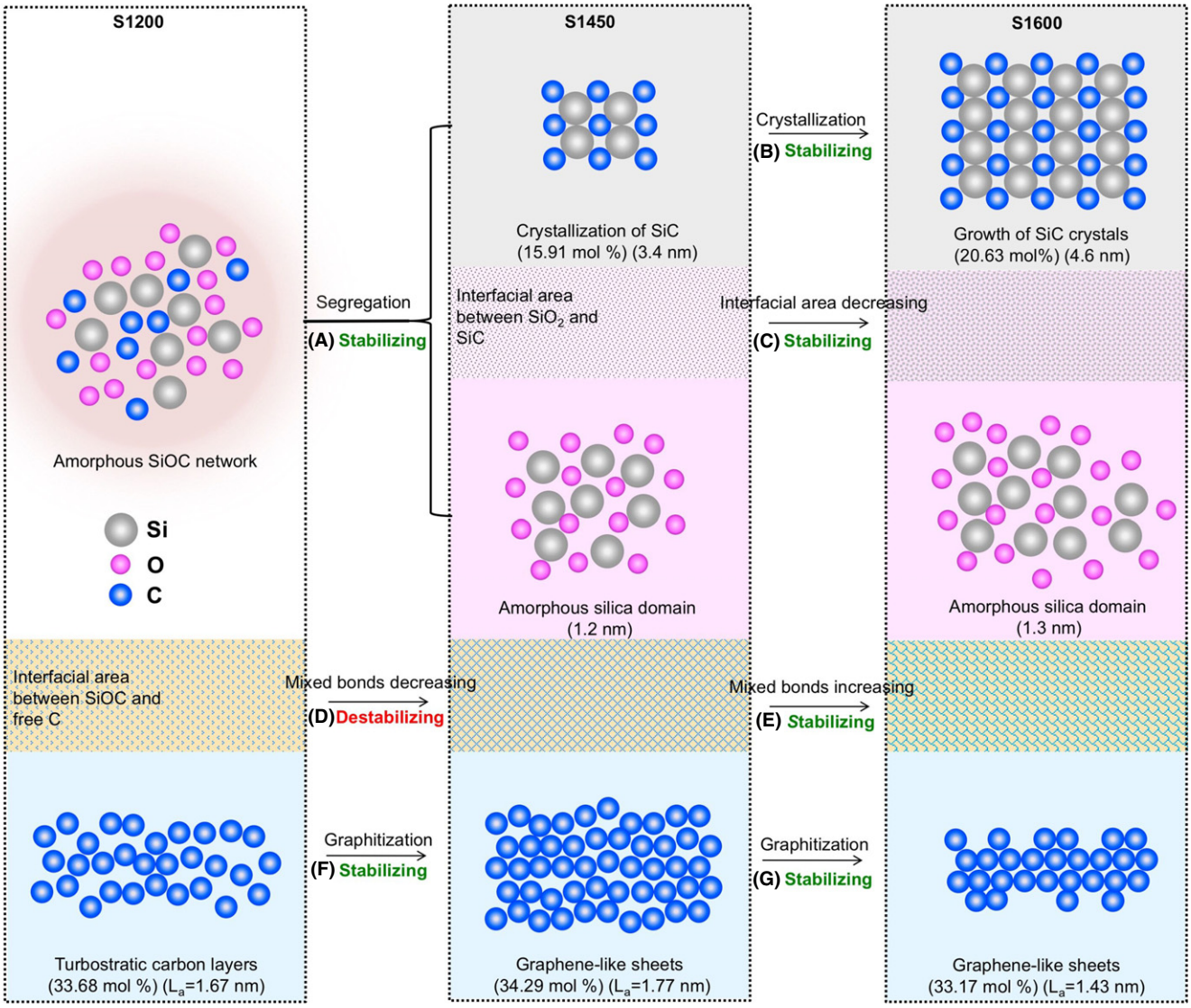

FIGURE 5 Structural evolutions of silica domains, SiC domains, free carbon regions, as well as dominant factors of stabilization and destabilization in S1200, S1450, and S1600 [Color figure can be viewed at wileyonlinelibrary.com]

the average coordination due to the incorporation of carbon atoms and the resulting high strain. Increasing temperature leads to rearrangement of Si–O and Si–C bonds, and favors the aggregation of SiO_4 and SiC_4 tetrahedra at the expense of mixed $SiO_{4-n}C_n$ tetrahedra. Simulation studies have demonstrated that a model comprising segregated SiC and SiO_2 and an interface between them has lower enthalpy than a model with homogeneously mixed bonds.[24] The segregation process enhances thermodynamic stability (Figure 5A). Continuous progress in heterogeneity as a function of raising the temperature and ordering of SiC_4 units eventually leads to precipitation and growth of nanosized SiC crystallites. Size and content of SiC crystals reach maximum value at 1600°C. The exothermic crystallization process reduces (makes more stable) the energy of the SiC nanodomain (Figure 5B). The growth of SiC nanocrystals is equivalent to a consumption of SiC_4 sites, accompanied by the exchange of Si–O and Si–C bonds between a SiC_4 site and a $SiO_{4-n}C_n$ site. The consumption of SiC_4 sites leads to the enrichment of newly formed Si–O and $SiO_{4-n}C_n$ sites toward the grain surface. The rather flexible Si–O bonds and remaining mixed bonds could relax constraints at the interfaces between SiC crystals and silica. Moreover, nanodomain growth is accompanied by a reduction in interfacial area and hence a decreased interfacial energy contribution to the enthalpy (Figure 5C). Crystallization of amorphous silica domains is limited by previously discussed kinetic factors. Therefore, with increasing temperature from 1200°C to 1600°C, the SiOC network region persists and tends to be stabilized in view of segregation of SiC and SiO_2, crystallization and growth of SiC, and decreased interfacial area between SiC and SiO_2.

The free carbon regions are intergrown with the amorphous SiOC domains. Additional energy could originate from distortions around sp^2 C (graphite-like) atoms and in

strain within C-segregation. Increasing temperature promotes larger agglomerates of carbon, especially graphitized carbon. Ordering of turbostratic carbon layers and growth of nanographitic domains to stacks of graphite-like layers improve energetic stability (Figure 5F,G). The carbon domain walls of graphene sheets could also slide to relieve the strain, reducing the energy relative to samples with lower graphitization degree. However, model calculations have shown that high excess energy introduced by interfacial regions is obvious even the free carbon is well ordered.[24] The embedding of carbon layers in the amorphous SiOC domains creates large amounts of interfaces. Significant excess energy originated from the covalent linkages of O–Si–C–C in the interfacial regions makes great contribution to the overall enthalpy of the system. It has been reported that mixed tetrahedral structural units play a key role in the thermodynamic stabilization by relaxing interfacial strain.[12] Destruction of the mixed bonded units makes the interfacial area energetically less stable, corresponding to a destabilizing process (Figure 5D). From ^{29}Si NMR data, S1200 has the highest concentration of mixed tetrahedral units accounting for 36.4% of the overall Si-containing units, which decreases to ~19.6% for S1450, and then increases to 24.8% for S1600. In addition, S1450 contains more free carbon than S1200, thus interfacial energy increases by creation of more carbon domains and formation of more interfacial regions. Hence, S1450 shows less energetic stability than S1200, reflecting less mixed bonding stabilization. Higher energetic stability for S1600 with respect to S1450 could be partially attributed to graphitization of carbon domains and increase of mixed bonds as seen from the NMR data. From the above analysis, it is reasonable to emphasize the role of mixed bonding between C, O, and Si atoms in the interfacial area in enhancing and controlling the thermodynamic stability of SiOC ceramics.

CS samples are composed of 0.12-8.52 mol% SiO_2, 1.56-6.55 mol% SiC, and 89.91-94.73 mol% excess carbon. Their energetic stability decreases as excess carbon content increases, suggesting that the existence of excess carbon does not by itself provide additional thermodynamic stability. Excess carbon in CS samples could be grouped into two categories: type I, carbon near the interfaces between the SiOC coating and the carbon fiber, and type II, carbon away from the interface. The formation of CS from SiOC and CBCFs involves incorporation of type II carbon and interactions between SiOC and type I carbon. Since type II carbon has little interaction with SiOC, the energetics of these CS samples could be governed more by the interactions introduced by type I carbon. The formation enthalpy becomes more endothermic as temperature increases from 1200°C to 1600°C, indicating decreasing energetic stability in the interfacial bonding region between SiOC and carbon fibers. This trend can be understood from their structural evolution. SiOC in CS1200 is amorphous. The concentration of silica domains in CS1200 is 8.52 mol%. Crystallization and growth of SiC grains is largely promoted by type I carbon in CS1450 and CS1600, accompanied by the consumption of almost all of silica (less than 0.17 mol% remaining). The interfacial energy could be lower in CS1200 as the more flexible silica units and mixed tetrahedral units could release interfacial strain. In contrast, the crystalline state imposes greater constraints on the configuration of chemical bonds at the interface.[32] Lack of stabilization of mixed bonds results in diminished energetic stability from growing SiC grain boundaries and interfaces between angular SiC grains and carbon, thus contributing high interfacial energy.

5 | CONCLUSIONS

Structural and energetic evolution of SiOC and SiOC-modified CBCFs were studied in detail. In summary, S1200 consists primarily of amorphous SiO_2, SiC, and nanodomains of sp^2 carbon with an interfacial region characterized by mixed bonding between O, C, and Si atoms. By increasing pyrolysis temperature, the amorphous silica clusters grow in size, amorphous SiC crystallize and grow in size, the mixed bonds decrease at 1450°C and then increase at 1600°C. Structural change in free carbon includes transformation from amorphous carbon to graphite. The graphitization degree and lateral size and amount of the free carbon regions reaches the maximum value at the pyrolysis temperature of 1450°C. Calorimetry results have demonstrated that mixed bonds play a key role in the thermodynamic stabilization of amorphous S1200, decrease of mixed bonds and increase of interfacial regions caused by more free carbon fragments in S1450 are mainly responsible for its smaller thermodynamic stability, while the growth of SiC crystals, graphitization of free carbon as well as increase of mixed bonds contribute to thermodynamic stabilization of S1600. In addition, CS sample becomes energetically *less* stable with increasing temperature and concomitant increase of excess carbon content.

ACKNOWLEDGMENTS

This work was supported by the National Natural Science Foundation of China (No. 51272206), the National Basic Research Program of China (973 Program) grant no.2015CB655200, and the Fundamental Research Funds for the Central University (xkjc2014009). M. N. thanks the China Scholarship Council for the State Scholarship Fund (No. 201506280144). The calorimetric studies at UC Davis were supported by the Fluid Interface Reactions, Structures & Transport, an Energy Frontier Research Center funded by the U.S. Department of Energy, Office of Science, and Office of Basic Energy Sciences under Award Number 4000134953.

REFERENCES

1. Xu T, Ma Q, Chen Z. High-temperature behavior of silicon oxycarbide glasses in air environment. *Ceram Int*. 2011;37(7):2555-2559.
2. Papendorf B, Ionescu E, Kleebe HJ, et al. High-temperature creep behavior of dense SiOC-based ceramic nanocomposites: microstructural and phase composition effects. *J Am Ceram Soc*. 2013;96(1):272-280.
3. Ionescu E, Balan C, Kleebe HJ, et al. High-temperature creep behavior of SiOC glass-ceramics: influence of network carbon versus segregated carbon. *J Am Ceram Soc*. 2014;97(12):3935-3942.
4. Guo X, Pei D, Zheng H, et al. Measurements of Schottky barrier at the low-k SiOC: H/Cu interface using vacuum ultraviolet photoemission spectroscopy. *Appl Phys Lett*. 2015;107(23):232905-232909.
5. Davies IJ, Rawlings RD. Microstructural investigation of low-density carbon-carbon composites. *J Mater Sci*. 1994;29(2):338-344.
6. Baxter R, Rawlings RD, Iwashita N, Sawada Y. Effect of chemical vapor infiltration on erosion and thermal properties of porous carbon/carbon composite thermal insulation. *Carbon*. 2000;38 (3):441-449.
7. Ahmed AS, Chlup Z, Dlouhy I, Rawlings RD, Boccaccini AR. Mechanical properties of low-density SiC-coated carbon-bonded carbon fiber composites. *Int J Appl Ceram Technol*. 2012;9(2):401-412.
8. Xu B, Hong C, Zhang QX, et al. Preparation of a multi-composition coating for oxidation protection of modified carbon-bonded carbon fiber composites by a rapid sintering method. *Surf Coat Technol*. 2015;270:109-116.
9. Niu M, Wang H, Su L, Zhang D, Shi J. Fabrication and properties of lightweight SiOC modified carbon-bonded carbon fiber composites. *Ceram Int*. 2016;42(9):10614-10618.
10. Wang K, Ma B, Li X, Wang Y, An L. Structural evolutions in polymer-derived carbon-rich amorphous silicon carbide. *J Phys Chem A*. 2015;119(4):552-558.
11. Mera G, Navrotsky A, Sen S, Kleebe HJ, Riedel R. Polymer-derived SiCN and SiOC ceramics–structure and energetics at the nanoscale. *J Mater Chem A*. 2013;1(12):3826-3836.
12. Varga T, Navrotsky A, Moats JL, et al. Thermodynamically stable SixOyCz polymer-like amorphous ceramics. *J Am Ceram Soc*. 2007;90(10):3213-3219.
13. Kleebe HJ, Turquat C, Sorarù GD. Phase separation in an SiCO glass studied by transmission electron microscopy and electron energy-loss spectroscopy. *J Am Ceram Soc*. 2001;84(5):1073-1080.
14. Liu C, Meng X, Zhang X, et al. High temperature structure evolution of macroporous SiOC ceramics prepared by sol-gel method. *Ceram Int*. 2015;41(9):11091-11096.
15. Morcos RM, Navrotsky A, Varga T, et al. Energetics of SixOyCz polymer-derived ceramics prepared under varying conditions. *J Am Ceram Soc*. 2008;91(9):2969-2974.
16. Chen J, King S, Muthuswamy E, Koryttseva A, Wu D, Navrotsky A. Thermodynamic stability of low-k amorphous SiOCH dielectric films. *J Am Ceram Soc*. 2016;99(8):2752-2759.
17. Niu M, Wang H, Wen J, Ma M, Fan X. Preparation and anti-oxidation properties of Si (O) C coated carbon-bonded carbon fiber composites. *RSC Adv*. 2015;5(65):52347-52354.
18. Leiser DB, Hsu MTS, Chen TS. Refractory oxidative-resistant ceramic carbon insulation. U.S. Patent 6,225,248, 2001.
19. Tavakoli AH, Armentrout MM, Narisawa M, Sen S, Navrotsky A. White Si–O–C ceramic: structure and thermodynamic stability. *J Am Ceram Soc*. 2015;98(1):242-246.
20. Navrotsky A. Progress and new directions in high temperature calorimetry revisited. *Phys Chem Miner*. 1997;24(3):222-241.
21. Li X, Zhang G, Tang K, Ostrovski O, Tronstad R. Carbothermal reduction of quartz in different gas atmospheres. *Metall Mater Trans B*. 2015;46(3):1343-1352.
22. Sorarù GD, Suttor D. High temperature stability of sol-gel-derived SiOC glasses. *J Sol Gel Sci Technol*. 1999;14(1):69-74.
23. Soraru GDD'andrea G, Campostrini R, Babonneau F, Mariotto G. Structural characterization and high-temperature behavior of silicon oxycarbide glasses prepared from sol-gel precursors containing Si–H bonds. *J Am Ceram Soc*. 1995;78(2):379-387.
24. Kroll P. Searching insight into the atomistic structure of SiCO ceramics. *J Mater Chem*. 2010;20(46):10528-10534.
25. Liu C, Pan R, Hong C, et al. Effects of Zr on the precursor architecture and high-temperature nanostructure evolution of SiOC polymer-derived ceramics. *J Eur Ceram Soc*. 2016;36(3):395-402.
26. Aguiar H, Serra J, González P, León B. Structural study of sol–gel silicate glasses by IR and Raman spectroscopies. *J Non-Cryst Solids*. 2009;355(8):475-480.
27. Widgeon S, Sen S, Mera G, Ionescu E, Riedel R, Navrotsky A. ^{29}Si and ^{13}C solid-state NMR spectroscopic study of nanometer-scale structure and mass fractal characteristics of amorphous polymer derived silicon oxycarbide ceramics. *Chem Mater*. 2010;22(23):6221-6228.
28. Babonneau F, Sorarú GD, Thorne KJ, Mackenzie JD. Chemical characterization of Si–Al–C–O precursor and its pyrolysis. *J Am Ceram Soc*. 1991;74(7):1725-1728.
29. Li JG, Tsai CY, Kuo SW. Fabrication and characterization of inorganic silver and palladium nanostructures within hexagonal cylindrical channels of mesoporous carbon. *Polymers*. 2014;6 (6):1794-1809.
30. Dresselhaus MS, Jorio A, Souza Filho AG, Saito R. Defect characterization in graphene and carbon nanotubes using Raman spectroscopy. *Philos Trans A Math Phys Eng Sci*. 2010;368:5355-5377.
31. Sadezky A, Muckenhuber H, Grothe H, Niessner R, Pöschl U. Raman microspectroscopy of soot and related carbonaceous materials: spectral analysis and structural information. *Carbon*. 2005;43(8):1731-1742.
32. Turnbull D, Jang J, Koch CC. Model for melting enthalpy of Sn in Ge–Sn composites. *J Mater Res*. 1990;5(8):1731-1732.

SUPPORTING INFORMATION

Additional Supporting Information may be found online in the supporting information tab for this article.

How to cite this article: Niu M, Wang H, Chen J, Su L, Wu D, Navrotsky A. Structure and energetics of SiOC and SiOC-modified carbon-bonded carbon fiber composites. *J Am Ceram Soc*. 2017;100:3693–3702. https://doi.org/10.1111/jace.14830